Applied Catalysis A: General xxx (2015) xxx–xxx

Contents lists available at ScienceDirect

Applied Catalysis A: General

journal homepage: www.elsevier.com/locate/apcata

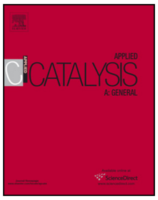

Reactivity and stability of supported Pd nanoparticles during the liquid-phase and gas-phase decarbonylation of heptanoic acid

Juan A. Lopez-Ruiz[a], Hien N. Pham[b], Abhaya K. Datye[b], Robert J. Davis[a,*]

[a] Department of Chemical Engineering, University of Virginia, Charlottesville, VA 22904-4741, USA
[b] Department of Chemical and Biological Engineering and Center for Microengineered Materials, University of New Mexico, Albuquerque, NM 87131, USA

ARTICLE INFO

Article history:
Received 8 September 2014
Received in revised form 14 January 2015
Accepted 20 January 2015
Available online xxx

Keywords:
Decarbonylation
Deoxygenation
Carboxylic acid
Heptanoic acid
Hexane
Hexene
Pd/C
Pd/SiO_2
Olefin
Paraffin

ABSTRACT

The liquid-phase and gas-phase decarbonylation of heptanoic acid over carbon- and silica-supported Pd nanoparticles was studied in a continuous-flow fixed-bed reactor at 573 K. The liquid-phase turnover frequency (TOF) under steady state conditions (>20 h) was very low at ≈0.00070 s^{-1}, presumably because of deposition of carbonaceous species and in some cases sintering of the metal particles, as revealed by H_2 chemisorption, X-ray diffraction and electron microscopy. The steady state rate was independent of the support composition, synthesis method, Pd loading (1–20 wt%), and acid concentration (0.1–6.6 M). Although the gas-phase reaction also led to deactivation of the supported Pd catalysts, extrapolation of the rate to initial time gave a TOF of ≈0.035 s^{-1} at 573 K. The liquid- and gas-phase reactions at low conversion levels were selective towards the formation of decarbonylation products such as CO and hexenes. Higher conversion levels resulted in the subsequent conversion of the primary decarbonylation products. *Post mortem* analysis of the catalysts revealed that concentrated, liquid-phase heptanoic acid at 573 K severely sintered the Pd nanoparticles supported on carbon but not those supported on silica. The Pd nanoparticles were able to maintain the high dispersion on carbon when exposed to low concentrations of liquid-phase heptanoic acid or gaseous heptanoic acid at 573 K.

1. Introduction

Biomass is an abundant, carbon-neutral alternative resource to fossil fuels for the production of fuels and chemicals. Processing of biomass presents a chemical challenge because it often contains excess oxygen that needs to be removed [1]. Dehydration, ketonization, decarbonylation and decarboxylation comprise a set of transformations collectively regarded as deoxygenation reactions. Organic acids, such as carboxylic acids, are biomass-derived molecules that can be readily converted to hydrocarbons by deoxygenation reactions. As shown in Scheme 1, linear carboxylic acids can be converted into linear olefins and paraffins by decarbonylation and decarboxylation, respectively. Ketonization is also an important reaction for the production of fine chemicals and fuels [2,3] in which two carboxylic acid molecules couple to form a symmetrical ketone, CO_2, and H_2O, as depicted in Scheme 2.

In our previous work, we studied the decarbonylation of heptanoic acid over Pt nanoparticles and reported low α-olefin selectivities because of olefin isomerization and sequential hydrogenation when the reaction was run at modest conversions [4]. At low conversions, however, decarbonylation was the primary reaction path [4]. Whereas Boda et al. [5] and Lugo-José et al. [6,7] also reported that decarbonylation was the main deoxygenation reaction over Pd catalysts, much of the deoxygenation literature [8–22] reports decarboxylation occurs when performing experiments in the presence of dihydrogen and solvent to inhibit catalyst deactivation and maximize the selectivity towards the formation of paraffins [17]. Discriminating between competing reaction paths based solely on the hydrocarbon products that are formed is difficult because alkenes are readily hydrogenated in the presence of H_2 and Pd. Nevertheless, Maier et al. speculated the active site on a Pd catalyst to be a Pd/H complex [23]. Interestingly, quantum chemical studies by Lamb et al. explored a potential mechanistic path to decarboxylate butanoic acid on a model Pd (1 1 1) surface [24], whereas Heyden and co-workers revealed a path to decarbonylate propanoic acid on Pd (1 1 1) [25,26].

Support composition and metal particle size have also been reported to affect the catalyst activity. For example, Lugo-José et al. studied the gas-phase decarbonylation of propanoic acid and

---

* Corresponding author at: Department of Chemical Engineering, University of Virginia, 102 Engineer's Way, PO Box 400741, Charlottesville, VA 22904-4741, USA. Tel.: +1 4349246284; fax: +1 4349822658.
E-mail address: rjd4f@virginia.edu (R.J. Davis).

http://dx.doi.org/10.1016/j.apcata.2015.01.032
0926-860X/

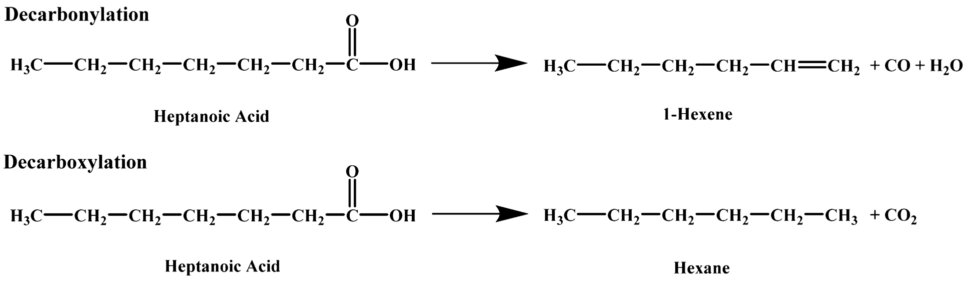

Scheme 1. Decarbonylation and decarboxylation of heptanoic acid.

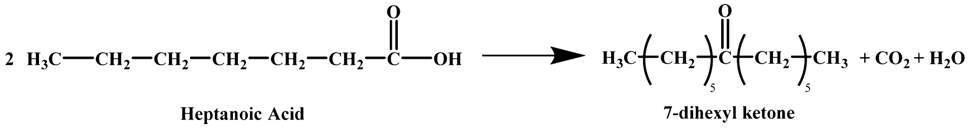

Scheme 2. Ketonization of heptanoic acid.

reported an increase in TOF by a factor of ≈32 when Pd nanoparticles were supported on silica instead of carbon [6], but Ford et al. reported a decrease in TOF of ≈3 fold when Pd nanoparticles were supported on silica instead of carbon during the liquid-phase operation [22]. In a different study, Lugo-José et al. reported during the gas-phase deoxygenation of propanoic acid at 473 K a constant TOF over Pd nanoparticles with sizes between 3.0 and 12 nm, but the TOF decreased by a factor of 3 when Pd nanoparticles of 1.9 nm were used instead [7]. In contrast, Simakova et al. reported an increase in TOF as the Pd nanoparticle size decreased from 6.1 to 2.3 nm during the liquid-phase deoxygenation of palmitic and stearic acid at 573 K [19].

Given the diversity of results reported for the conversion of carboxylic acids over supported Pd catalysts, which seem to depend on both catalyst type and reaction conditions, we studied systematically the decarbonylation and decarboxylation of heptanoic acid over a wide variety of supported Pd catalysts in a continuous-flow fixed-bed reactor. This study highlights the effect of reaction conditions on catalyst stability and reactivity. In particular, the effects of support type, Pd impregnation method, Pd weight loading, acid conversion, reaction phase, and acid concentration on the activity, product selectivity, and catalyst stability were examined.

2. Experimental methods

2.1. Catalyst synthesis

The catalysts were prepared by incipient wetness impregnation (IWI) using aqueous solutions of tetraamminepalladium (II) nitrate, $(NH_3)_4Pd(NO_3)_2$ (Sigma–Aldrich) to obtain 1, 5, 10, and 20 wt% Pd loadings on Norit activated carbon (ROX 0.9), respectively. Prior to impregnation, Norit carbon particles were crushed and sieved between 180 and 425 μm. After impregnation of the desired metal precursor solution, the catalyst was dried in air at 393 K overnight. Palladium (II) acetate, $Pd(OCOCH_3)_2$, was used to prepare catalysts by the alcohol reduction (AR) method, as described by Benavidez et al. [27], to obtain a 5 wt% loading on Norit activated carbon, Vulcan carbon (XC-72), and Davisil silica 636. Vulcan carbon and Davisil silica were used as received. All of the dried solids were reduced in H_2 (GTS-Welco 99.999%) flowing at 100 $cm^3\ min^{-1}$. The temperature of reduction was increased at 1 $K\ min^{-1}$ from room temperature to 623 K, and held isothermally for 3 h. The catalysts were then cooled, exposed to air, and stored in a vial.

2.2. Dihydrogen chemisorption

The Pd dispersion was measured by H_2 chemisorption performed on a Micromeritics ASAP 2020 system. Each catalyst was evacuated at 573 K for 10 h under vacuum followed by heating to 623 K at a rate of 1 $K\ min^{-1}$ after which it was reduced with flowing H_2 (GTS-Welco 99.999%) at 623 K for 3 h. Following reduction, the catalyst sample was evacuated at 573 K and cooled in vacuum to 373 K to prevent β-phase hydride formation during chemisorption. The amount of metal on the surface was evaluated by the total amount of H_2 adsorbed extrapolated to zero pressure, assuming a stoichiometric relationship between H_2 to metal of 1:2 (i.e. H/Pd = 1). The average spherical Pd particle size from chemisorption, which is analogous to the surface-weighted average Pd particle size [28], was estimated from the inverse of the Pd dispersion (i.e. inverse of the fraction of metal exposed) [29].

2.3. Dinitrogen physisorption

The specific surface area and pore size were measured by N_2 physisorption using a Micromeritics ASAP 2020. The samples were evacuated for 180 min at 373 K prior to the N_2 physisorption, after which adsorption isotherms were measured at 77 K. The Brunauer–Emmett–Teller (BET) and the Barrett–Joyner–Halenda (BJH) methods were used to determine the specific surface area and the pore size, respectively.

2.4. X-ray diffraction

Powder X-ray diffraction (XRD) analysis from $2\theta = 20$ to 100° was carried out on a X'Pert Pro MPD with monochromatic Cu Kα-radiation using a step size of 0.05°. The Scherrer analysis [30] was used to determine the average Pd crystallite size according to Eq. (1):

$$D_{\text{Pd Crystallite}} = \frac{\kappa\lambda}{\beta\cos\theta} \tag{1}$$

where $D_{\text{Pd Crystallite}}$ represents an average Pd crystallite size analogous to the volume-weighted apparent Pd crystallite size [28], κ represents the shape factor (e.g. 0.9 for this case), λ represents the X-ray wavelength (1.54056 Å for the Cu Kα-radiation), β represents the full width at half maximum (FWHM) of a specific diffraction peak, and θ represents the diffraction angle. Using the JADE 2010 software, we did a profile fit to all of the Pd diffraction peaks, and the average Pd crystallite size was determined over multiple peaks.

Please cite this article in press as: J.A. Lopez-Ruiz, et al., Appl. Catal. A: Gen. (2015), http://dx.doi.org/10.1016/j.apcata.2015.01.032

2.5. Electron microscopy

Transmission electron microscopy (TEM) was performed to determine the Pd particle size (D_P) on an FEI Titan operated at 300 keV in bright field mode and on a JEOL 2010F operated at 200 KeV in STEM high-angle annular dark-field (HAADF) mode. Catalyst samples were deposited on a SPI holey-carbon coated Cu grid after being dispersed in ethanol [31]. For each fresh sample, four TEM images were used to count Pd particle sizes and 40–50 particles were measured per image. The average Pd particle size was calculated for each image followed by the mean and standard deviation of the average sizes. The surface-weighted average Pd particle size was calculated using $\sum D_{P,i}^3 / \sum D_{P,i}^2$, and the volume-weighted average Pd particle size was calculated using $\sum D_{P,i}^4 / \sum D_{P,i}^3$.

2.6. Catalytic conversion of heptanoic acid

The catalytic decarbonylation/decarboxylation of heptanoic acid (Sigma–Aldrich ≥99.50%) was performed in a fixed-bed tubular reactor described previously [4]. In summary, the reactor was loaded with 50–500 mg of catalyst pellets supported on a glass wool plug. Fresh catalyst was used for each experiment because of the irreversible deactivation of the catalyst as described in our previous work with Pt catalysts. After loading the reactor, the system was purged for 60 min with 200 $cm^3 min^{-1}$ of N_2 (GTS-Welco 99.999%) at atmospheric pressure to remove dioxygen from the system and the pressure was increased to 45 bar to perform a leak test and then depressurized. The temperature was then increased at 1 K min^{-1} to the desired reduction temperature, 623 K, under 100 $cm^3 min^{-1}$ of H_2 (GTS-Welco 99.999%) and held isothermally for 3 h at atmospheric pressure. The reactor was finally cooled to the desired reaction temperature, 573 K, and purged for 60 min in 200 $cm^3 min^{-1}$ of N_2 (GTS-Welco 99.999%). Then, the pressure was increased to the desired reaction condition with 200 $cm^3 min^{-1}$ of N_2 (GTS-Welco 99.999%). The reactor system was operated at two different pressures, 40 bar for liquid-phase operation and 1 bar for gas-phase operation.

For the "pure" acid experiments, the feed mixture was composed of 95 wt% heptanoic acid (Sigma–Aldrich ≥99.50%) and 5 wt% dodecane (Sigma–Aldrich anhydrous 99.00%) as an internal standard. Tetradecane (Sigma–Aldrich anhydrous 99.90%) was used as a diluent to prepare feeds with different heptanoic acid concentration (50, 25, 10, 7.5, 5, and 2.5 mol%). The feed was then pumped in the reaction system using a syringe pump operating at different liquid flow rates (0.01–1.0 $cm^3 min^{-1}$). The acid feed mixtures passed through a heated zone before entering the catalytic reactor. A schematic of the reactor can be found in the paper by Lopez-Ruiz and Davis [4].

The outlet of the reactor was connected to an air cooled condenser maintained at room temperature to remove the condensable products, such as hexane, 1-hexene, hexenes, 7-tridecanone, dodecane, tetradecane, and unreacted heptanoic acid, from the product stream. The liquid-phase sample was analyzed by a gas chromatograph (GC 7890 A) equipped with a ZB-FFAP column (length 45 m × 0.538 mm) and a flame ionization detector (FID). The product gas was continuously removed from the condenser using 5 $cm^3 min^{-1}$ N_2 (GTS-Welco 99.999%) as a purge gas. The outlet gas of the condenser was fed to an on-line gas chromatograph (HP 5890 Series II) equipped with a packed column, ShinCarbon ST 80/100, and a thermal conductivity detector (TCD) for detection of N_2, CO, CO_2 and any other light hydrocarbons (if any).

A series of control experiments was performed to determine the background conversion of the system at our typical reaction conditions (573 K, 40 bar for liquid-phase operation or 1 bar for gas-phase operation, 250 mg of catalyst, and 0.01 $cm^3 min^{-1}$ of liquid feed composed of 95 wt% heptanoic acid and 5 wt% dodecane). In the absence of catalyst, no conversion of heptanoic acid was observed. However, when Norit or Vulcan carbon support was used, a background conversion of ≈2 and 1%, respectively, was detected. No conversion was observed over the silica support.

2.7. Post mortem catalyst characterization

The spent samples were recovered from the reactor, washed with 25 mL of methanol and sonicated in a methanol solution for 30 min to remove weakly adsorbed reactant and products from the surface of the catalyst. After sonication, the solids were recovered by filtration and dried overnight in air at 400 K. The spent samples were characterized by H_2 chemisorption, N_2 physisorption, XRD, and TEM to determine the effect of reaction conditions on the catalyst structure and adsorption capacity.

2.8. Calculations of rates

As described in our previous work, the turnover frequency (TOF) was calculated as the rate of formation of the products referred to the number of surface metal atoms evaluated on a freshly prepared catalyst [4]. The main components in the gas-phase were CO and CO_2, whereas 1-hexene, 2- and 3-hexenes (i-hexenes), hexane, 7-tridecanone, and heptanoic acid were the main compounds in the liquid-phase. Some minor amounts of heavier unknown products were also detected in the liquid-phase products (which accounted for ≈0.4% of the total detected liquid product).

The liquid-phase TOF was calculated using the rate of formation of the products after 20 h of reaction, after which the liquid-phase reaction was at a steady state, normalized to the number of surface metal atoms evaluated on a fresh catalyst. The liquid-phase TOF was therefore calculated as [(rate of production after 20 h of reaction (mol s^{-1}) hexane + 1-hexene + i-hexenes + 2 × moles of 7-tridecanone)/(mol of surface metal on a fresh catalyst counted by H_2 chemisorption)].

During gas-phase operation, the catalyst deactivated exponentially with time during the first 3 h of reaction. Thus, an initial TOF was calculated by extrapolating the log of the reaction rate to $t = 0$ h. The initial TOF was calculated as [(rate of production (mol s^{-1}) of hexane + 1-hexene + i-hexenes + 2 × moles of 7-tridecanone)/(mol of surface metal on a fresh catalyst counted by H_2 chemisorption)].

The deoxygenation conversion is defined here as the formation rates of the major products divided by the feed rate of reagent. Thus, the deoxygenation conversion was calculated as [(rate of production (mol s^{-1}) of hexane + 1-hexene + i-hexenes + 2 × moles of 7-tridecanone)/(moles of heptanoic acid fed (mol s^{-1}))].

The product selectivity was defined as the moles of a product formed divided by the total moles of products present in the same phase (liquid or gas). Three different sets of product selectivity were calculated, the selectivity to carbon oxides (CO and CO_2), i.e. CO selectivity [(rate of CO)/(rate of CO + rate of CO_2)], the selectivity of α-olefin relative to all olefin produced for 1-hexene and hexenes, i.e. relative α-olefin selectivity [(rate of 1-hexene)/(rate of 1-hexene + i-hexenes)], and the selectivity to deoxygenation products for mainly hexane, 1-hexene, i-hexenes, and 7-tridecanone, i.e. selectivity of hexane [(rate of hexane)/(rate of hexane + 1-hexene + i-hexenes + 2 × moles of 7-tridecanone)].

The carbon balance was defined as the moles of carbon identified after reaction divided by the total moles of carbon fed to the reactor, i.e. carbon balance [(rate (mol s^{-1}) of unreacted heptanoic acid × 7 + hexane × 6 + 1-hexene × 6 + i-hexenes × 6 + 7-tridecanone × 13 + CO + CO_2)/(moles of heptanoic acid fed × 7 (mol s^{-1}))]. For the experiments reported here, the carbon balance was between 98 and 99%.

Please cite this article in press as: J.A. Lopez-Ruiz, et al., Appl. Catal. A: Gen. (2015), http://dx.doi.org/10.1016/j.apcata.2015.01.032

Table 1
Summary of the catalyst characterization and reactivity results for Pd catalysts synthesized by alcohol reduction (AR) during the liquid-phase reaction at 573 K.

Catalysts	Pd dispersion[a] (%)	TEM			XRD average Pd crystallite size[c] (nm)	Surface area[d] ($m^2 g^{-1}$)	Pore size[e] (nm)	Liquid-phase TOF[f] (s^{-1})	CO selectivity[g] (%)
		Number average Pd particle size[b] (nm)	Surface average Pd particle size (nm)	Volume average Pd particle size[b] (nm)					
5 wt% Pd/SiO_2	43	2.1 ± 0.1	2.3[a]/2.3[b] N.C.[h]	2.4 N.C.[h]	N.C.[i] N.C.[i]	500	6.2	0.00069	69
5 wt% Pd/Norit C	20	2.2 ± 0.1	5.0[a]/3.0[b] N.C.[h]	3.6 N.C.[h]	N.C.[i] 8.5[k]	1460	N.D.[j]	0.00069	71
5 wt% Pd/Vulcan C	11	3.4 ± 0.5	9.1[a]/5.6[b] N.C.[h]	7.0 N.C.[h]	10 12[k]	210	8.8	0.00071	91

[a] Result estimated from H_2 chemisorption of the fresh catalyst sample, using nominal Pd loading.
[b] Result estimated from TEM of the fresh catalyst sample.
[c] Result estimated from Scherrer analysis of XRD pattern.
[d] Result estimated using N_2 physisorption and the BET method on the fresh catalyst sample.
[e] Result estimated using N_2 physisorption and the BJH method on the fresh catalyst sample.
[f] Result estimated using rates of heptanoic acid conversion after 20 h of reaction.
[g] Result estimated using rates of carbon oxide formation after 20 h of reaction.
[h] N.C., not calculated, both large Pd crystallites and Pd nanoparticles are present in the spent catalyst sample.
[i] N.C., not calculated, because of a lack of Pd diffraction features on the fresh and spent catalyst sample.
[j] N.D., not determined, both micropores and mesopores are present on this sample.
[k] Result estimated from Scherrer analysis of XRD pattern of the spent catalyst sample.

2.9. *Mass transfer limitations*

In our previous work with heptanoic acid decarbonylation over carbon-supported Pt nanoparticles at identical conditions [4], the extent of internal and external mass transfer limitations was estimated using the Weisz–Prater criterion [32]. For the highest observed rate over Pt nanoparticles with a liquid-phase TOF ≈ 0.005 s^{-1}, the criterion suggested that the system was not mass transfer limited with respect to heptanoic acid. In the current work, we observed much lower liquid-phase rates over Pd nanoparticles, TOF ≈ 0.0007 s^{-1}, which suggests that the system is not influenced by mass transfer limitations either.

The Weisz–Prater criterion [32] assumes first-order reaction kinetics; however, as discussed in Section 3.4, the reaction appears to be operating under saturation conditions, zero-order reaction kinetics, which are not affected by concentration gradients resulting from mass transfer limitations. For this reason, the Weisz–Prater criterion cannot be used to assess the mass transfer limitations under our working conditions. Instead, the potential role of mass transfer limitations will be evaluated by changing pore size of the catalyst and the Pd weight loading, as discussed in Sections 3.1 and 3.2 respectively.

3. Results and discussion

3.1. *Effect of support and impregnation method during the liquid-phase operation*

In our previous study [4], low metal dispersion was achieved with 5 wt% Pt synthesized by an incipient wetness impregnation (IWI) method on low surface area supports such as Vulcan carbon and silicon carbide. For this reason, we decided to use an alcohol reduction (AR) method to deposit Pd nanoparticles on Vulcan carbon and silica. Since high dispersion of metal can be achieved with Norit carbon as support, Pd was added to Norit carbon by either incipient wetness impregnation or alcohol reduction to test the influence of preparation method.

Catalysts composed of Pd particles loaded on the various supports were characterized by N_2 physisorption, H_2 chemisorption, XRD, and TEM, and the results are summarized in Tables 1 and 2 for samples synthesized by AR and IWI, respectively. The mean and standard deviation calculated from TEM analysis, based on random sampling of Pd size distribution, show good statistics, and therefore, uniform size distribution in the fresh Pd samples. Although the dispersion of Pd on Pd/SiO_2 corresponded to a particle size consistent with the observed surface average particle size evaluated by TEM (2.3 nm), the particle size of the Pd/Norit C samples and Pd/Vulcan C derived from chemisorption were larger than the surface average particle sizes observed by TEM. Evidently, there was a discrepancy between the surface average Pd diameter estimated by TEM and the surface average Pd particle size estimated by H_2 chemisorption for samples with lower dispersion, especially Pd/Vulcan C. Therefore, the catalysts were examined by X-ray diffraction. Fig. 1 provides evidence for Pd crystallites on Vulcan C, even before reaction, which likely accounts for the low dispersion of Pd measured by H_2 chemisorption. There is an unusual peak shape at 40° 2θ for spent 5 wt% Pd/Norit C. However, the sample was reproduced several more times with consistent results and may be due to sample displacement error. Whereas TEM of the fresh Pd/Vulcan (Fig. 2) revealed a volume average Pd particle size of 7.0 nm (Table 1), the Scherrer analysis of the fresh Pd/Vulcan sample revealed an average Pd crystallite size of 10 nm, which is also more consistent

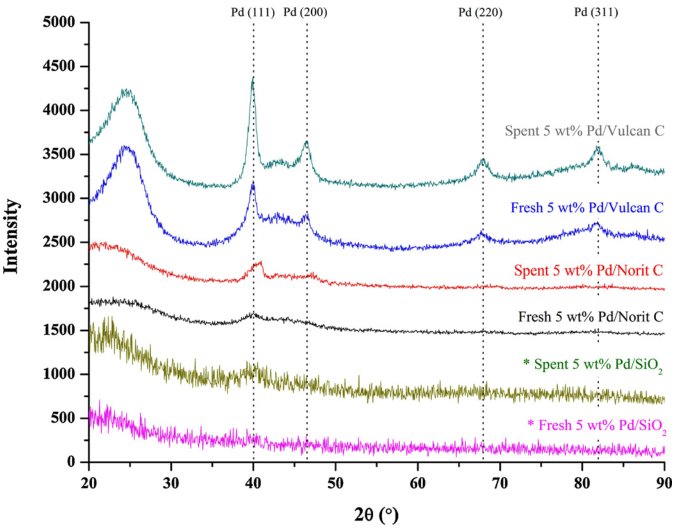

Fig. 1. Comparison of the XRD patterns of 5 wt% Pd/Norit C, 5 wt% Pd/Vulcan C, and 5 wt% Pd/SiO_2 prepared by alcohol reduction (AR) before (fresh) and after (spent) liquid-phase reaction at 573 K. The patterns were offset for clarity. '*' indicates that the diffraction patterns were expanded (×10) for clarity.

Please cite this article in press as: J.A. Lopez-Ruiz, et al., Appl. Catal. A: Gen. (2015), http://dx.doi.org/10.1016/j.apcata.2015.01.032

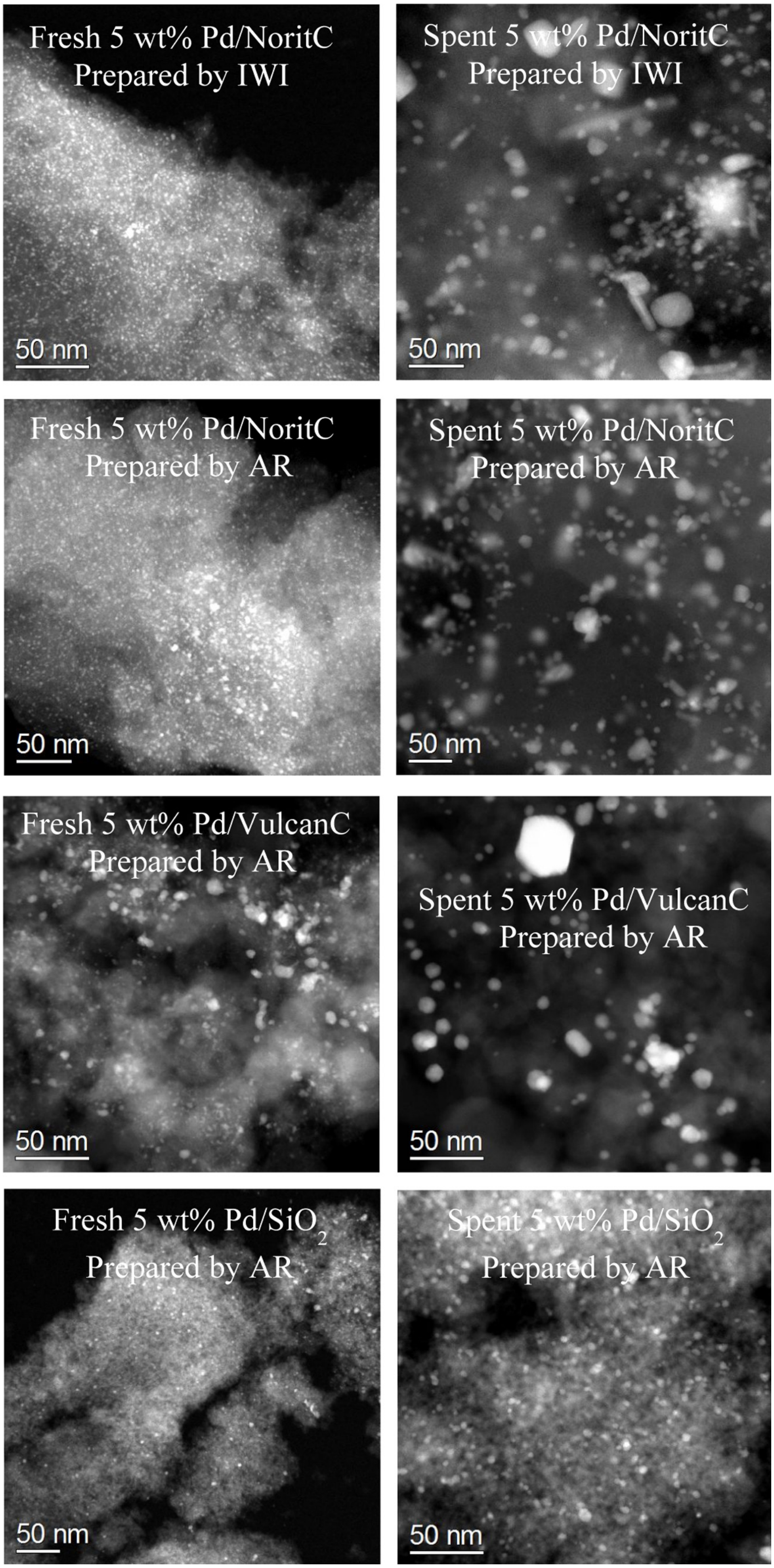

Fig. 2. High-angle annular dark field STEM images of fresh (left) and spent (right) Pd catalysts used for the liquid-phase decarbonylation of heptanoic acid at 573 K.

Please cite this article in press as: J.A. Lopez-Ruiz, et al., Appl. Catal. A: Gen. (2015), http://dx.doi.org/10.1016/j.apcata.2015.01.032

Table 2
Summary of catalysts characterization and reactivity results for Pd catalysts synthesized by incipient wetness impregnation (IWI) during the liquid-phase reaction at 573 K.

Catalyst	Reaction temp. (K)	Pd dispersion[a] (%)	TEM			XRD average Pd crystallite size[c] (nm)	Surface area[d] ($m^2 g^{-1}$)	Liquid-phase TOF[e] (s^{-1})	CO selectivity[f] (%)
			Number average Pd particle size[b] (nm)	Surface average Pd particle size (nm)	Volume average Pd particle size[b] (nm)				
1 wt%	Fresh	25	1.9 ± 0.2	4.0[a]/2.2[b]	2.3	N.C.[h]	1460	–	–
Pd/Norit C	573	0.0	–	N.C.[g]	N.C.[g]	N.C.[h]	495	0.00071	70
5 wt%	Fresh	25	2.1 ± 0.0	4.0[a]/2.2[b]	2.3	N.C.[h]	1450	–	–
Pd/Norit C	573	0.0	–	N.C.[g]	N.C.[g]	7.9	510	0.00069	67
10 wt%	Fresh	25	2.4 ± 0.1	4.0[a]/2.7[b]	2.8	4.9	1400	–	–
Pd/Norit C	573	1.2	–	N.C.[g]	N.C.[g]	7.8	540	0.00069	60
20 wt%	Fresh	24	2.5 ± 0.0	4.2[a]/2.8[b]	2.9	5.6	1460	–	–
Pd/Norit C	573	1.7	–	N.C.[g]	N.C.[g]	15	530	0.00068	54

[a] Result estimated from H_2 chemisorption on the fresh and spent catalyst samples, using nominal Pd loading.
[b] Result estimated from TEM on the fresh catalyst samples.
[c] Result estimated from the Scherrer analysis of XRD pattern on the fresh and spent catalyst samples.
[d] Result estimated using N_2 physisorption and the BET method on the fresh and spent catalyst samples.
[e] Result estimated using rates of heptanoic acid conversion after 20 h of reaction.
[f] Result estimated using rates of carbon oxide formation after 20 h of reaction.
[g] N.C., not calculated, both large Pd crystallites and Pd nanoparticles are present in the spent catalyst sample.
[h] N.C., not calculated, because of a lack of Pd diffraction features on the fresh and spent catalyst sample.

with the surface average Pd particle size derived from H_2 chemisorption. Evidently, whereas the particle size evaluated by TEM undercounted the larger Pd crystallites, the Scherrer analysis and H_2 chemisorption accounted for them. We assume the discrepancy between the Pd particle size derived from TEM, Scherrer analysis, and H_2 chemisorption observed in the Pd/Norit C samples can be explained in the same way.

After liquid-phase reaction, both of the carbon-supported catalysts had much more intense diffraction peaks associated with Pd, most likely the result of metal sintering that occurred under the liquid-phase reaction conditions, as reported for Pt catalysts [4]. Figs. 1 and 2 indicate growth of Pd particles on all the carbon-supported catalysts. The Scherrer analysis of the spent catalysts revealed that the average Pd crystallite size of the Pd/Vulcan C increased from 10 to 12 nm. Similarly, the average Pd crystallite size of the spent Pd/Norit prepared by AR (Table 1) and IWI (Table 2) increased to 8.5 and 7.9 nm, respectively, compared to the volume average Pd particle size estimated by TEM of the fresh samples, 3.6 and 2.3 nm respectively. Interestingly, the silica-supported catalyst still showed highly dispersed Pd nanoparticles, as depicted in Fig. 2. This result suggests that silica might be a better support than carbon for stabilizing metal particles under the harsh reaction conditions. Since all of the catalysts had very low rate after 20 h of liquid-phase (TOF ≈ 0.00070 s^{-1}), the large variation in final metal particle size does not explain the deactivation.

Figs. 3 and 4a show the liquid-phase product selectivity after 20 h of reaction for the 5 wt% Pd catalyst synthesized by AR and IWI, respectively. The two 5 wt% Pd/Norit C catalysts exhibited similar

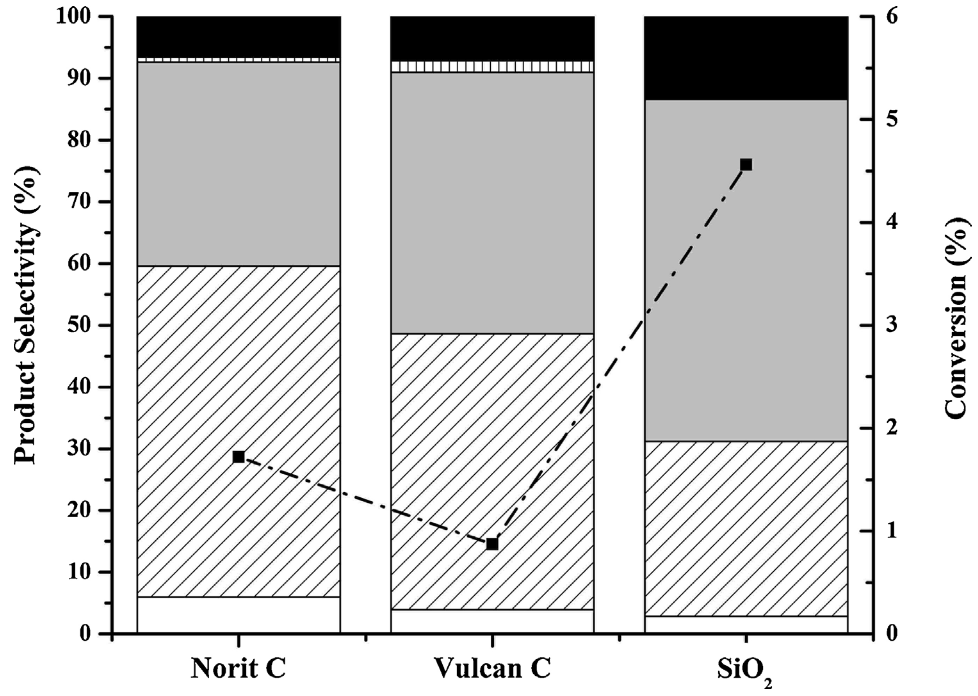

Fig. 3. Effect of support on product selectivity and conversion during the liquid-phase decarbonylation of heptanoic acid at 573 K, 40 bar, and 0.01 $cm^3 min^{-1}$ of liquid feed composed of 95 wt% heptanoic acid and 5 wt% dodecane. The product selectivity (%) is represented with bars and can be read on the left axis. □ represents 1-hexene, ▨ represents 2 and 3-hexenes, ▒ represents hexane, ▥ represents 7-tridecanone, and ■ represents the unknown products. The black squares represent conversion (%) and can be read on the right axis. The background conversion of the carbon supports was removed for clarity. These results were recorded after 20 h of reaction.

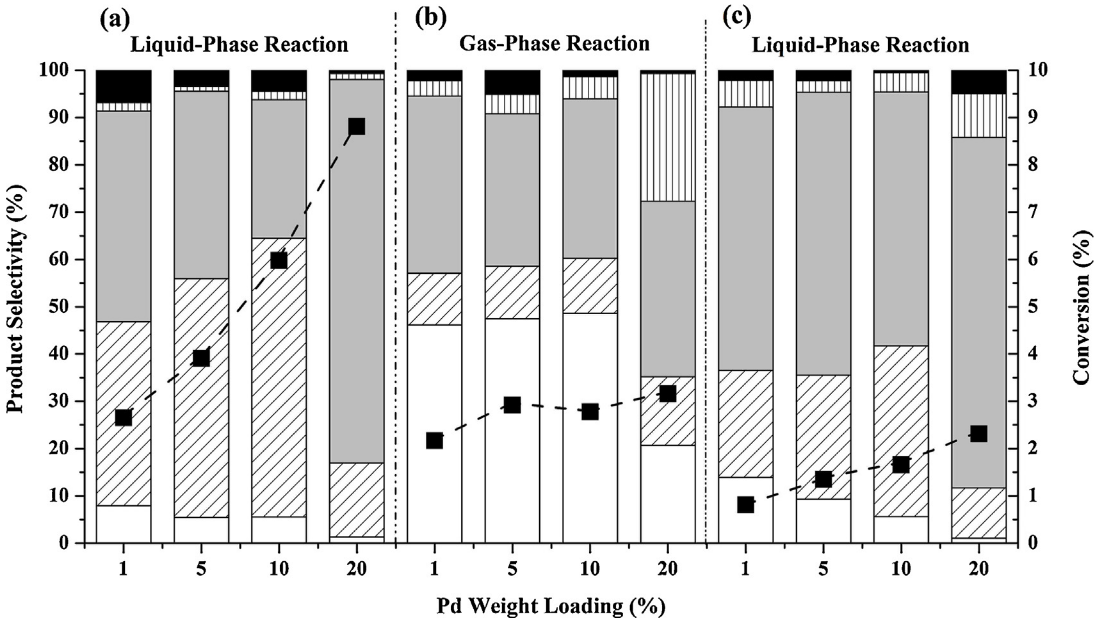

Fig. 4. Effect of Pd loading on Norit C on product selectivity and conversion during the (a) liquid-phase reaction at 40 bar, (b) subsequent gas-phase reaction at 1 bar and (c) subsequent liquid phase reaction at 40 bar, of heptanoic acid at 573 K, and 0.01 cm^3 min^{-1} of liquid feed composed of 95 wt% heptanoic acid and 5 wt% dodecane. The product selectivity (%) is represented with color bars and can be read on the left axis. □ represents 1-hexene, ▨ represents 2 and 3-hexenes, ▣ represents hexane, ▥ represents 7-tridecanone, and ■ represents the unknown products. The black squares represent conversion (%) and can be read on the right axis. The background conversion of the carbon support was removed for clarity.

conversion level and product selectivity during reaction of heptanoic acid, with the main liquid-phase products being hexane and hexenes. Evidently, the impregnation method and metal precursor did not influence the catalytic performance or stability of the resulting Pd nanoparticles. The variation of conversion with 5 wt% Pd sample in Fig. 3 was likely the result of the different initial dispersion of the catalysts, with Pd/Vulcan C having the lowest initial dispersion. Nevertheless, the major liquid-phase products formed over all of the samples were hexenes and hexane.

The system was tested for internal mass transfer limitations by changing the pore size of the support from microporous (<2 nm) in the case of Norit carbon up to 8.8 nm for Vulcan carbon. As shown in Table 1, the liquid-phase steady state TOF remained constant independent of the pore size, which suggests that the system was not affected by internal mass transfer limitations.

Because silica is unstable at high temperatures in the presence of high concentrations of water (a product of the reaction) [33], and high dispersion of Pd was not successfully achieved on Vulcan C, we focused additional efforts on the performance of Pd/Norit C.

3.2. Effect of metal loading and reaction pressure

In a previous study, we reported the liquid-phase TOF for Pt/Norit C at 573 K to be independent of Pt loading at a value of ≈0.005 s^{-1} [4]. As reported in Tables 1 and 2, Pd/Norit C converted heptanoic acid at 573 K in the liquid-phase with a TOF of ≈0.0007 s^{-1}, which is about an order of magnitude less than that for Pt/Norit C under identical conditions [4]. Because of the low activity of Pd in the liquid-phase reaction, the metal loading of Pd was increased to 20 wt% to minimize the relative contribution of the Norit C support to the catalytic evaluation. The results from the catalyst characterization and reaction testing of the higher loaded samples are summarized in Table 2.

The catalyst characterization of the fresh catalysts synthesized by IWI revealed that the surface area (≈1500 m^2 g^{-1}) and Pd dispersion (≈25%) was independent of Pd loading. The characterization of the spent catalysts revealed a severe loss of surface area to ≈500 m^2 g^{-1} and almost a complete loss of exposed Pd measured by H_2 chemisorption. Apparently the evacuation step for surface area determination and the reduction step for H_2 chemisorption were not sufficient to regenerate the high surface area and chemisorption capacity of the fresh catalyst. These results were consistent with the observations previously reported by Simakova et al. [19], Immer et al. [20], and Ping et al. [34], who studied the decarboxylation of carboxylic acids over Pd catalysts. We suspect that adsorption of carbonaceous materials in the pores and on the Pd was the major cause of deactivation, as previously reported by Ping et al. [34,35], because the reaction over Pd/SiO_2 was also very low after 20 h of reaction and was not accompanied by Pd particle growth.

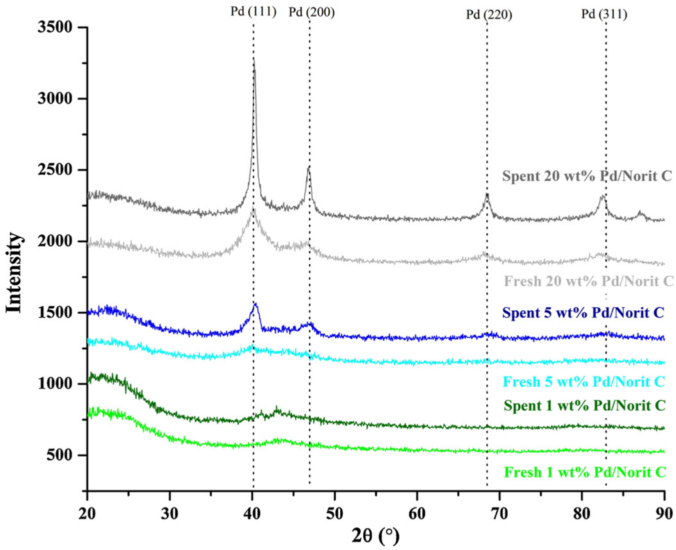

Fig. 5. Comparison of the XRD patterns of 1, 5, and 20 wt% Pd/Norit C prepared by incipient wetness impregnation before (fresh) and after (spent) liquid-phase reaction of heptanoic acid at 573 K. The patterns were offset for clarity.

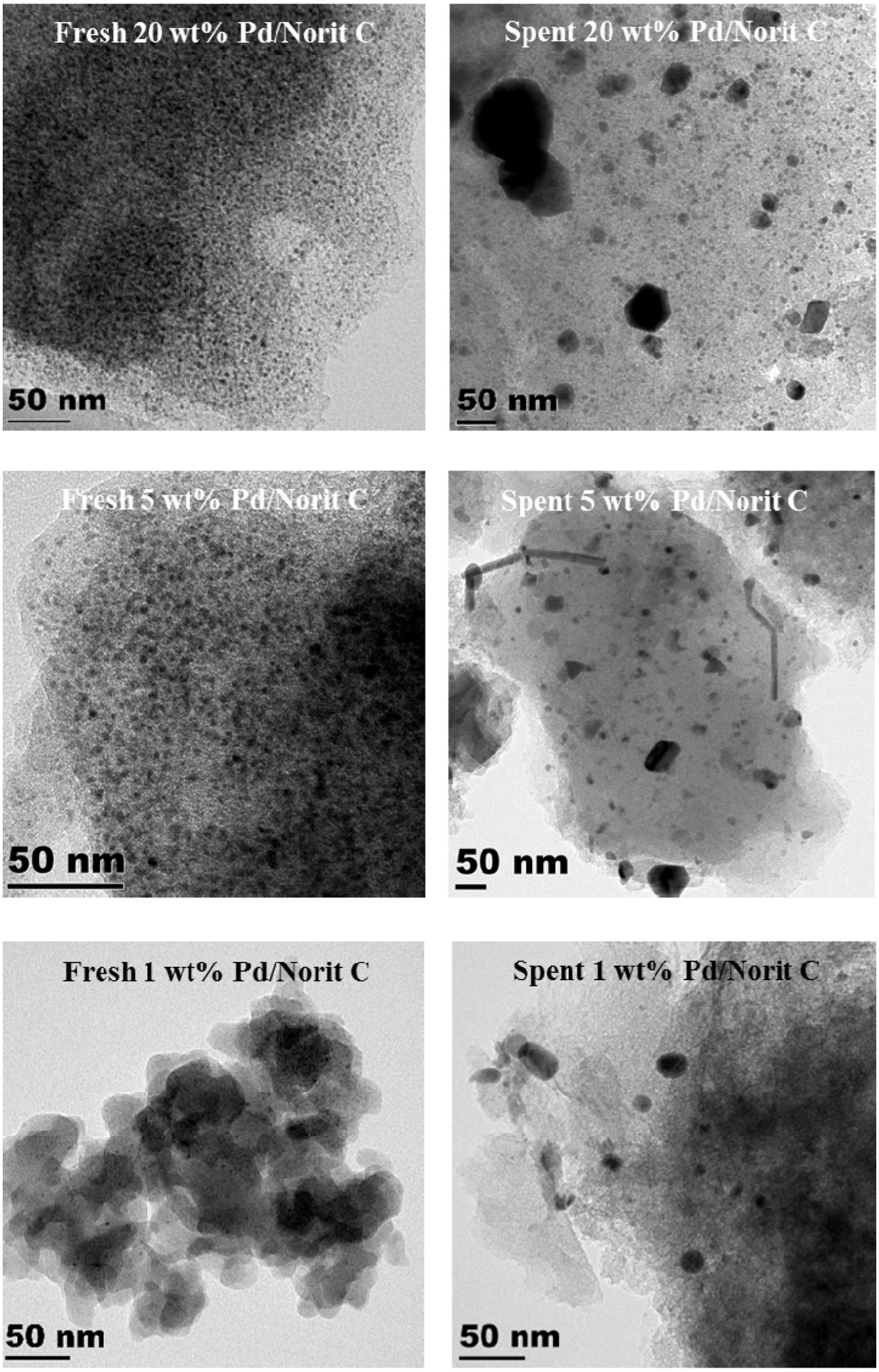

Fig. 6. Bright field HRTEM images of fresh (left) and spent (right) Pd/Norit C samples after the liquid-phase decarbonylation of heptanoic acid at 573 K.

Figs. 5 and 6 show the XRD patterns and electron micrographs, respectively, of the Pd/Norit C catalysts with various Pd loadings, before and after reaction. We observed slight shifts in the XRD Pd peaks possibly due to sample displacement error. Nonetheless, significant Pd particle growth was observed at every loading on Norit C, as revealed by the micrographs in Fig. 6. The XRD patterns are consistent with the growth of particles after reaction on the higher loaded samples (5–20 wt%). The lack of significant Pd diffraction features on the 1 wt% Pd sample was likely because of the low metal loading. At higher loadings, we start to observe XRD peaks (Fig. 5) even on the fresh samples with highly dispersed Pd nanoparticles as revealed in Fig. 6. Also, we observed the same discrepancy discussed in the previous section among the Pd particle sizes derived from TEM, XRD, and H_2 chemisorption of the fresh catalyst samples. Results in Table 2 might suggest that the average Pd particle size of the fresh and spent samples increases as the Pd weight loading increases. For example, the Scherrer analysis revealed that the average Pd crystallite size of 10 wt% Pd/Norit C increased from 4.9

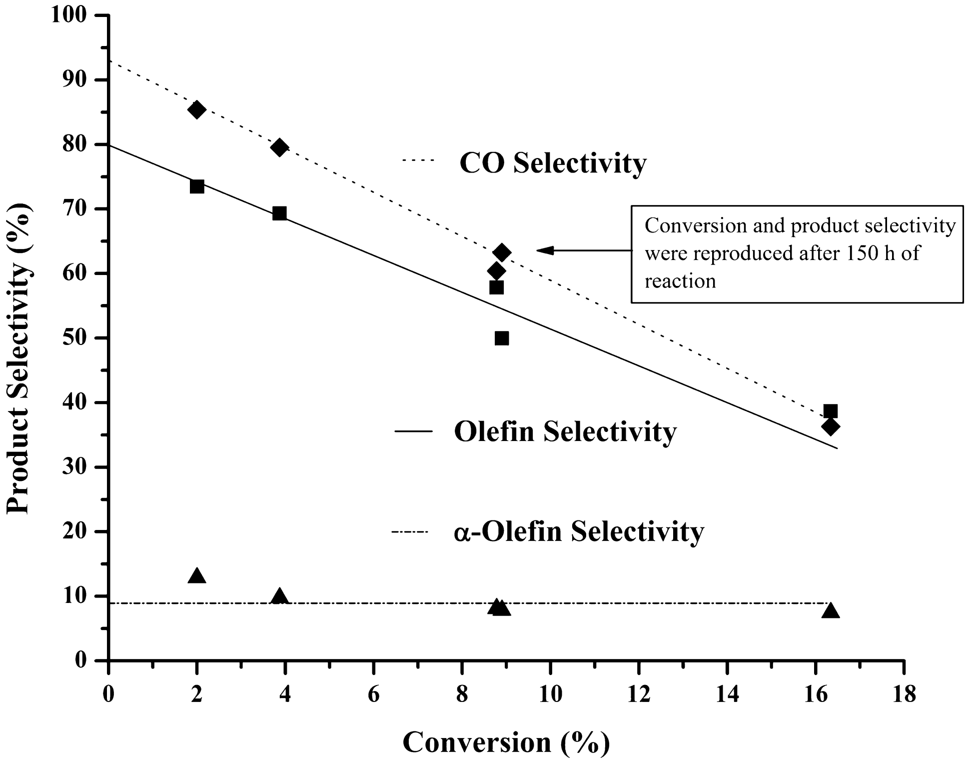

Fig. 7. Dependence of product selectivity on liquid-phase conversion of heptanoic acid over 10 wt% Pd/Norit C at 573 K and 40 bar. ■ represents the selectivity to olefins (1-, 2- and 3-hexenes) decarbonylation products, olefins, in the liquid product. ♦ represents the carbon oxide selectivity to CO. ▲ represents the selectivity to α-olefin relative to all olefins in the liquid product. These results were recorded after 20 h of reaction.

to 7.8 nm after reaction and the average Pd crystallite size of 20 wt% Pd/Norit C increased from 5.6 to 15 nm.

The product distribution during the liquid-phase conversion of heptanoic acid over Pd catalysts with low metal loading favored the formation of hexenes (1-, 2- and 3-hexenes) and CO, but was difficult to distinguish from that attributed to the carbon support (Fig. 4a). The catalyst with the highest weight loading (20 wt% Pd) showed a different product distribution favoring the formation of hexane and CO_2. As the liquid-phase conversion increased because of the added Pd, the selectivity towards the formation of 1-hexene decreased. This observation was consistent with our previous work performed on Pt/Norit C, in which we found rapid bond isomerization of terminal olefins over the Pt at our reaction conditions [4].

After 25 h of liquid-phase operation, the system was depressurized to allow for operation with gas-phase heptanoic acid. During the gas-phase operation (Fig. 4b), the selectivity towards the α-olefin was higher than that observed during the liquid-phase experiments, but the catalyst deactivated, as previously reported [4]. The deactivation was more severe with catalysts having higher Pd loading (10 and 20 wt% Pd). After operating in gas-phase for 25 h, the system was re-pressurized to liquid-phase reaction conditions (Fig. 4c). The catalytic activity of the various Pd catalysts did not recover to their initial steady state liquid-phase levels, indicating an irreversible change of the catalysts during the gas-phase operation.

The reported values for turnover frequency (TOF) of carboxylic acid conversion over Pd generally ranged 0.01–0.96 s^{-1} for batch reaction at 573 K [15,16,20,21] and from 0.004 to 0.027 s^{-1} for fixed-bed operation at 543 K [8,10]. Although these values are substantially greater than those reported in this work, differences in reaction conditions such as not co-feeding H_2 and feeding nearly pure carboxylic acid might account for the differences in TOF. For example, Murzin and co-workers [9,10,14–16,19] as well as Lamb and co-workers [20–22] studied the liquid-phase conversion of carboxylic acids in the presence of H_2 over Pd catalysts and reported TOFs from 0.01 to 0.1 s^{-1} at 573 K. Characterization of our spent catalysts revealed substantial loss in H_2 chemisorption capacity, suggesting our reaction conditions generally deactivated the catalyst.

The constancy of the measured liquid-phase steady state TOF, ≈0.0007 s^{-1}, on catalysts with different concentration of active sites (different Pd weight loading) is consistent with the absence of artifacts from transport limitations under our reaction conditions, as previously reported [4].

3.3. *Effect of liquid-phase conversion on product selectivity*

To minimize the impact of support activity on the results, we studied the liquid-phase conversion of heptanoic acid at 573 K over 10 wt% Pd/Norit C at various space velocities to explore the influence of conversion on the product distribution. With a constant loading of catalyst, the feed flow rate was varied from 0.005 to 0.05 $cm^3\ min^{-1}$ over a period of 150 h (≈370 turnovers) to obtain a range of conversion values. At the end of experiment, the catalyst returned to the initial reaction condition to check for deactivation. Fig. 7 summarizes the effect of conversion on product selectivity achieved by varying the space velocity. The reproducibility of the initial conversion (≈9%) to that achieved at identical conditions after 150 h of reaction confirms that long term deactivation was not significant during the course of the experiment.

Fig. 7 shows a very strong correlation of the product selectivity to conversion. Extrapolation of the product selectivities to zero conversion indicates ≈90% of the carbon oxides is CO and 80% of the liquid-phase products are hexenes. Therefore, the main reaction path during the liquid-phase conversion of heptanoic acid over Pd/Norit C at 573 K is decarbonylation, which is consistent with previously reported results over Pt/Norit C [4]. Fig. 7 also shows a low selectivity to α-olefin, between 7 and 12%, across the

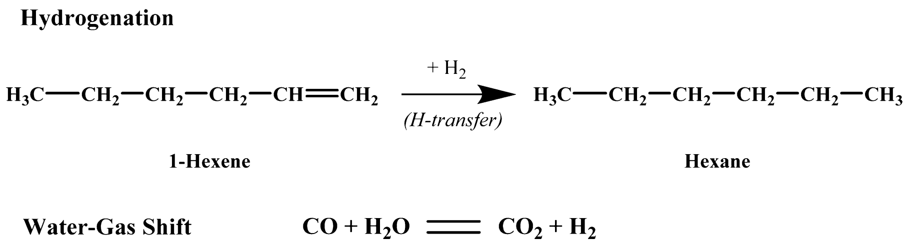

Scheme 3. Some possible side reactions during the conversion of heptanoic acid.

conversion range. As discussed earlier, metal-catalyzed double bond isomerization of 1-hexene to 2- and 3-hexenes occurs rapidly on Pd.

The selectivity for hexenes was lower than the selectivity for CO, indicating the existence of a side reaction that hydrogenated hexenes into hexane. In previous work with heptanoic acid decarbonylation over supported Pt [4], a higher olefin selectivity compared to CO selectivity was observed, with the loss of CO being attributed to the water-gas shift reaction. Scheme 3 shows some possible side reactions that take place during the conversion of heptanoic acid. Since the water-gas shift activity of Pd is less than that of Pt, as reported by Grenoble and Estadt [36], we suspect the hydrogen involved in the hydrogenation of the hexenes to hexane in the current work originated from the adsorption and decomposition of the organic acid on the catalyst.

Nevertheless, the results in Fig. 7 clearly support the idea that decarbonylation is the primary reaction of heptanoic acid on Pd under our experimental conditions. The fact that the fraction of CO exceeds the fraction of hexenes at low conversions suggests that olefin hydrogenation occurs readily on the catalysts and is independent of the water-gas shift reaction.

3.4. Gas-phase operation

Because liquid-phase heptanoic acid causes growth of Pd particles on the carbon support, we decided to explore the gas-phase conversion over 10 wt% Pd/Norit C without exposing the catalyst to liquid acid. The reactivity results summarized in Fig. 8 reveal that the catalyst deactivated severely during the first 2 h of reaction (Fig. 8a), and that the deactivation was followed by changes in product selectivity. Initially, we observed an acid conversion of 16.5%, with the CO selectivity (Fig. 8b) being similar to that of hexenes

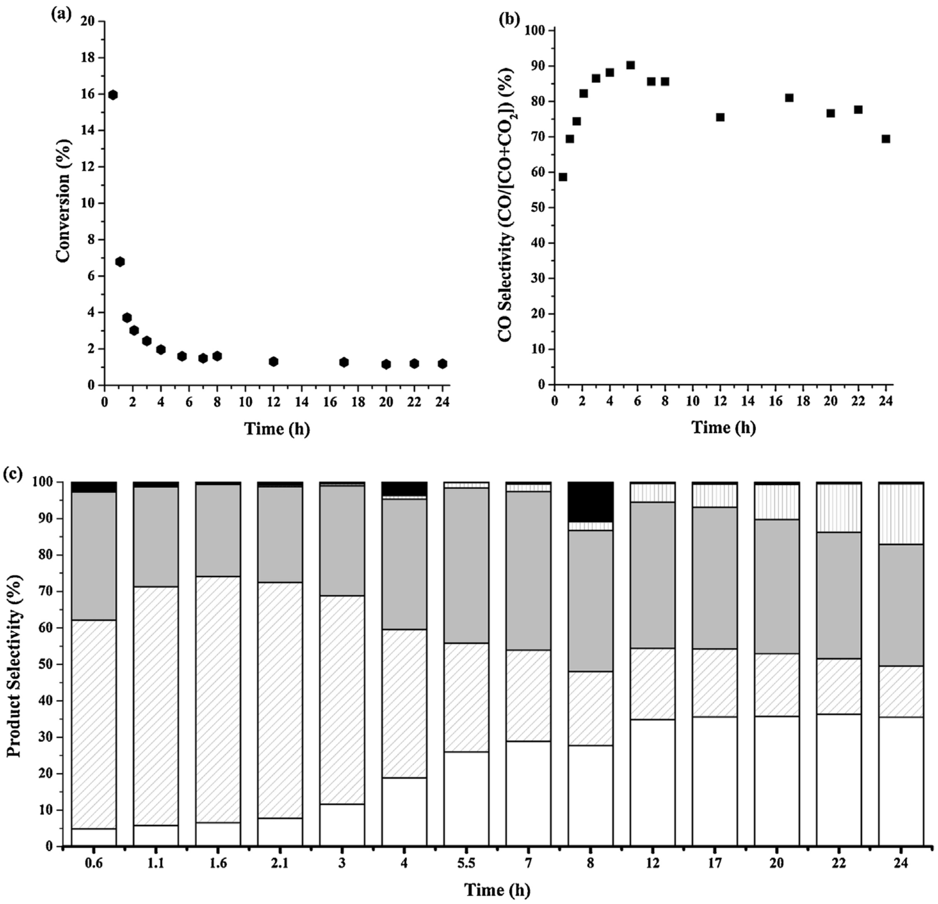

Fig. 8. Time evolution of the (a) conversion, (b) CO selectivity, and (c) liquid product selectivity during the gas-phase decarbonylation of heptanoic acid over 10 wt% Pd/Norit C at 573 K, 1 bar, and 0.05 cm^3 min^{-1} of liquid feed composed by 95 wt% heptanoic acid (6.6 M) and 5 wt% dodecane. The product selectivity in (c) is represented with bars where □ represents 1-hexene, ▨ represents 2 and 3-hexenes, ▒ represents hexane, ▥ represents 7-tridecanone, and ■ represents the unknown products.

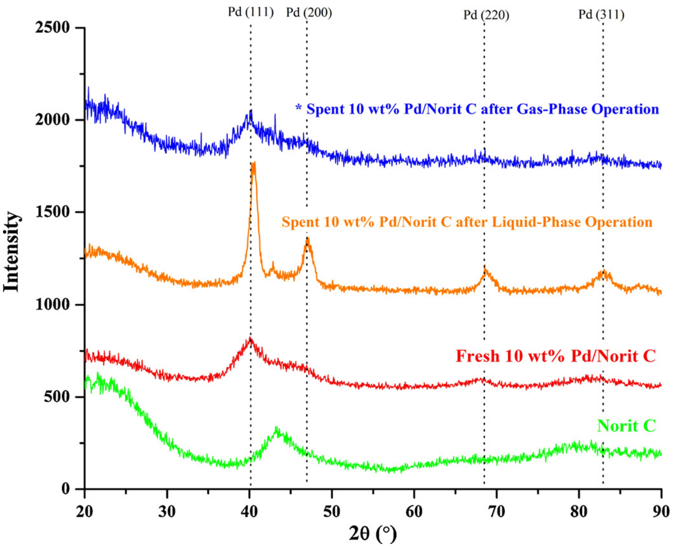

Fig. 9. Comparison of the XRD patterns of 10 wt% Pd/Norit C before and after reactions at 573 K. The patterns were offset for clarity. '*' indicates that the diffraction pattern was expanded (×3) for clarity.

(Fig. 8c). The 1-hexene selectivity was very low, ≈5%, indicating rapid double bond isomerization.

As the catalyst deactivated, the CO selectivity increased to a maximum of 90% before decreasing to 70% by the end of the experiment (Fig. 8b). Similarly, the hexenes selectivity increased to 70% before decreasing to 50%. The decrease of CO selectivity at long times was most likely the result of the ketonization reaction, which was observed after 4 h of reaction. Ketonization of heptanoic acid produces CO_2 and 7-tridecanone (Scheme 2). The hexane produced during the reaction could not be produced entirely by direct decarboxylation because of the lack of CO_2 produced relative to CO as provided in Fig. 8b and c. Evidently, some hydrogenation of hexenes to hexane occurred. Regarding the olefin selectivity, up to 35% terminal olefin was observed after long times on stream (Fig. 8c), which is consistent with decarbonylation followed by some double bond isomerization.

Extrapolation of the conversion to $t = 0$ h allows for an estimation of the initial rate unaffected by deactivation. Using this method, we obtained a gas-phase TOF = 0.035 s^{-1}, which was ≈50 times faster than that of the liquid-phase TOF and similar to the values reported by others. As speculated in the previous section and suggested by the *post mortem* catalyst characterization with H_2 chemisorption, the liquid-phase TOF reported here was very likely affected by severe catalyst deactivation, which explains the order of magnitude difference between the liquid-phase TOF reported here and the literature [9,10,14–16,19–22].

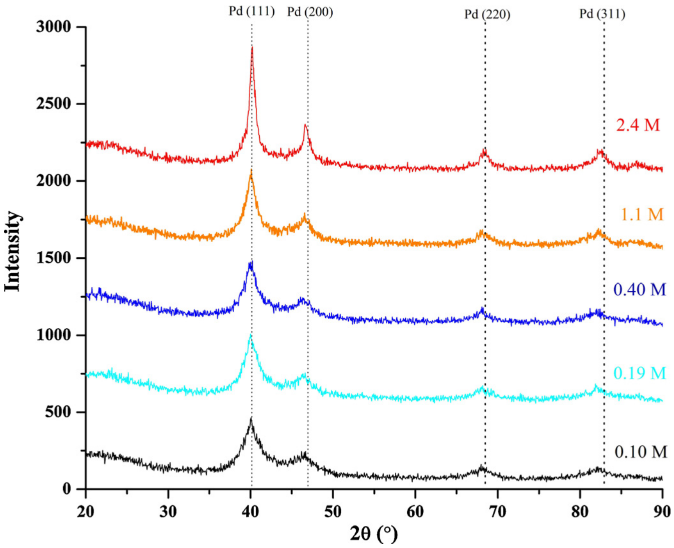

Fig. 11. Comparison of the XRD patterns of 20 wt% Pd/Norit C after the liquid-phase operation at 573 K with different acid concentrations. The patterns were offset for clarity.

Lugo-José et al. reported a TOF of 0.00017 s^{-1} for the gas-phase decarbonylation of propanoic acid over Pd/C at 473 K and an activation barrier of ≈72 kJ mol^{-1} [6]. The Arrhenius equation was used to extrapolate their rate to 573 K and revealed a TOF of ≈0.0042 s^{-1}. While this extrapolated value is an order of magnitude lower than the initial gas-phase Pd TOF reported here, it is similar to our final gas-phase Pd TOF of 0.0011 s^{-1}. This may suggest that the catalysts of Lugo-José et al. [6] suffered from partial deactivation even though H_2 (20 vol%) was fed during that study.

Figs. 9 and 10 compare the X-ray diffraction patterns and electron micrographs, respectively, of the spent catalysts from the gas-phase reaction. Even though the catalyst deactivated severely during the first 2 h of reaction, XRD and TEM revealed that the Pd nanoparticles remained well dispersed after the gas-phase reaction. Evidently, sintering of Pd on the carbon support occurs only when operating in the liquid-phase acid. Severe deactivation occurred during gas-phase operation, not because of sintering, but presumably because of strongly held side products or carbonaceous species on the metal surface.

Since gas-phase operation apparently prevented severe Pd particle growth, we decided to investigate the stability of Pd particles in various concentrations of liquid heptanoic acid. Figs. 11 and 12 present results from exposing 20 wt% Pd/Norit C to progressively lower liquid concentrations of reacting acid at 573 K. After 20 h of reaction, the catalyst in dilute acid (0.19 M) appeared to be more

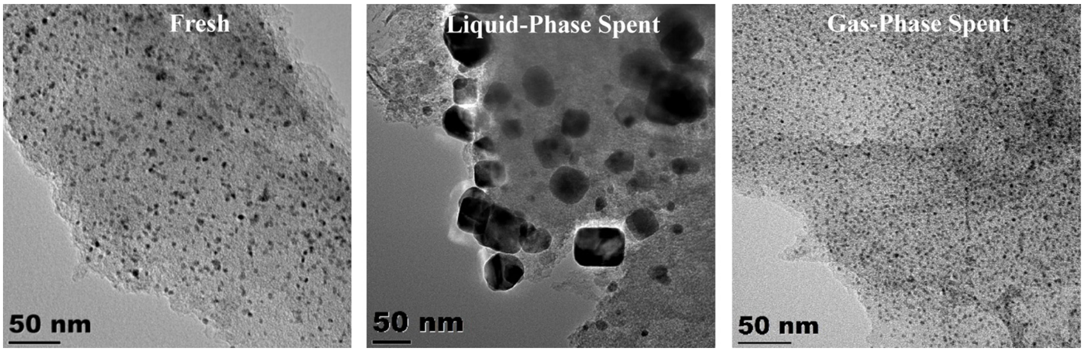

Fig. 10. Bright field HRTEM images of 10 wt% Pd/Norit C before reaction (left), recovered after liquid-phase operation (middle), and recovered after gas-phase operation (right) at 573 K.

Please cite this article in press as: J.A. Lopez-Ruiz, et al., Appl. Catal. A: Gen. (2015), http://dx.doi.org/10.1016/j.apcata.2015.01.032

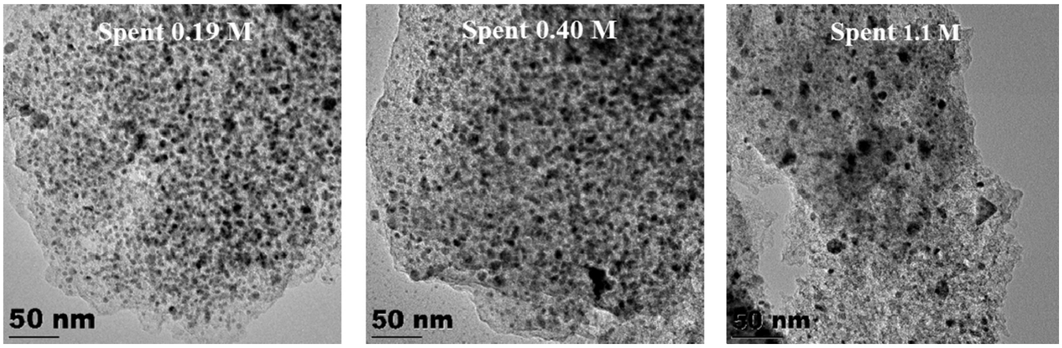

Fig. 12. Bright field HRTEM images of 20 wt% Pd/Norit C after the liquid-phase operation at 573 K with different acid concentrations.

dispersed than one in more concentrated acid (1.1–6.6 M), confirming the hypothesis that concentrated liquid acid is detrimental to Pd particle dispersion on carbon. Interestingly, the liquid-phase steady state TOF at 573 K (≈0.0007 s^{-1}) was independent of acid concentration from 0.1 to 6.6 M. This result indicated that the system was operating in the zero-order regime and is in agreement with the observations reported by Mäki-Arvela et al. [10]. Observed zero order behavior is consistent with a lack of mass transport artifacts with respect to the acid.

4. Conclusions

Palladium nanoparticles were supported on Davisil silica 636, Vulcan carbon and Norit carbon, characterized by H_2 chemisorption, N_2 physisorption, X-ray diffraction, electron microscopy (before and after reaction,) and evaluated in the liquid- and gas-phase conversion of heptanoic acid at 573 K. Decarbonylation was the primary reaction of heptanoic acid on Pd, producing hexene, CO and water (not measured). In liquid-phase operation, some hydrogenation of the olefins to hexane and conversion of CO to CO_2 was observed, especially at higher conversions. Rapid conversion of α-olefin to internal olefin was also observed in the liquid- and gas-phase operation at high conversion. A steady state TOF of 0.00070 s^{-1} at 573 K was obtained for the liquid-phase conversion of heptanoic acid over Pd, which was independent of synthesis method, support composition, Pd loading, and acid concentration. The very low TOF was a result of severe catalyst deactivation. Operation in gas-phase allowed for extrapolation of rates to initial time in an effort to evaluate the TOF on a fresh catalyst surface. An initial gas-phase TOF of 0.035 s^{-1} was estimated from the initial rate at 573 K over supported Pd.

Post mortem characterization of the catalysts revealed a decrease of surface area and almost complete loss of H_2 chemisorption capacity after the liquid-phase operation, which accounts for the low steady state rate under those conditions. X-ray diffraction and electron microscopy revealed that Pd nanoparticles supported on carbon sintered substantially during the liquid-phase operation in nearly pure acid. In contrast, carbon-supported Pd nanoparticles were quite stable during gas-phase reaction. Likewise, the sintering of carbon-supported Pd nanoparticles in the liquid-phase was less significant at low acid concentrations. Silica-supported Pd nanoparticles maintained a high dispersion during the liquid-phase operation at high acid concentrations.

Acknowledgements

This material is based upon work supported by the National Science Foundation (NSF) under Award No. EEC-0813570. Any opinions, findings, and conclusions or recommendations expressed in this material are those of the author(s) and do not necessarily reflect the views of the NSF. We acknowledge discussions with Professor Matthew Neurock at the University of Virginia. We also gratefully acknowledge Mr. Matthew Schneider at the University of Virginia for his help with the bright field TEM.

References

[1] A.J. Ragauskas, C.K. Williams, B.H. Davison, G. Britovsek, J. Cairney, C.A. Eckert, W.J. Frederick, J.P. Hallett, D.J. Leak, C.L. Liotta, J.R. Mielenz, R. Murphy, R. Templer, T. Tschaplinski, Science 311 (2006) 484–489.
[2] M. Renz, Eur. J. Org. Chem. 2005 (2005) 979–988.
[3] C.A. Gaertner, J.C. Serrano-Ruiz, D.J. Braden, J.A. Dumesic, J. Catal. 266 (2009) 71–78.
[4] J.A. Lopez-Ruiz, R.J. Davis, Green Chem. 16 (2014) 683–694.
[5] L. Boda, G. Onyestyák, H. Solt, F. Lónyi, J. Valyon, A. Thernesz, Appl. Catal. A-Gen. 374 (2010) 158–169.
[6] Y.K. Lugo-José, J.R. Monnier, C.T. Williams, Appl. Catal. A-Gen. 469 (2014) 410–418.
[7] Y.K. Lugo-José, J.R. Monnier, A. Heyden, C.T. Williams, Catal. Sci. Technol. 4 (2014) 3909–3916.
[8] S. Lestari, P. Mäki-Arvela, H. Bernas, O. Simakova, R. Sjöholm, J. Beltramini, G.Q.M. Lu, J. Myllyoja, I. Simakova, D.Y. Murzin, Energ. Fuel 23 (2009) 3842–3845.
[9] S. Lestari, I. Simakova, A. Tokarev, P. Mäki-Arvela, K. Eränen, D.Y. Murzin, Catal. Lett. 122 (2008) 247–251.
[10] P. Mäki-Arvela, M. Snåre, K. Eränen, J. Myllyoja, D.Y. Murzin, Fuel 87 (2008) 3543–3549.
[11] B. Rozmysłowicz, P. Mäki-Arvela, S. Lestari, O.A. Simakova, K. Eränen, I.L. Simakova, D.Y. Murzin, T.O. Salmi, Top. Catal. 53 (2010) 1274–1277.
[12] M. Snåre, I. Kubičková, P. Mäki-Arvela, K. Eränen, J. Wärnå, D.Y. Murzin, Chem. Eng. J. 134 (2007) 29–34.
[13] M. Snåre, I. Kubičková, P. Mäki-Arvela, K. Eränen, D.Y. Murzin, Ind. Eng. Chem. Res. 45 (2006) 5708–5715.
[14] I. Simakova, B. Rozmysłowicz, O.A. Simakova, P. Mäki-Arvela, A. Simakov, D.Y. Murzin, Top. Catal. 54 (2011) 460–466.
[15] I. Kubičková, M. Snåre, K. Eränen, P. Mäki-Arvela, D. Murzin, Catal. Today 106 (2005) 197–200.
[16] P. Mäki-Arvela, I. Kubičková, M. Snåre, K. Eränen, D.Y. Murzin, Energ. Fuel 21 (2007) 30–41.
[17] M. Snåre, I. Kubičková, P. Mäki-Arvela, D. Chichova, K. Eränen, D.Y. Murzin, Fuel 87 (2008) 933–945.
[18] S. Lestari, P. Mäki-Arvela, I. Simakova, J. Beltramini, G.Q.M. Lu, D.Y. Murzin, Catal. Lett. 130 (2009) 48–51.
[19] I. Simakova, O. Simakova, P. Mäki-Arvela, A. Simakov, M. Estrada, D.Y. Murzin, Appl. Catal. A-Gen. 355 (2009) 100–108.
[20] J.G. Immer, H.H. Lamb, Energ. Fuel 130 (2010) 5291–5299.
[21] J.G. Immer, M.J. Kelly, H.H. Lamb, Appl. Catal. A-Gen. 375 (2010) 134–139.
[22] J.P. Ford, J.G. Immer, H.H. Lamb, Top. Catal. 55 (2012) 175–184.
[23] W.F. Maier, W. Roth, I. Thies, P.v. Rague Schleyer, P. Ragukschleyer, R. Schleyer, Chem. Ber. 115 (1982) 808–812.
[24] H.H. Lamb, L. Sremaniak, J.L. Whitten, Surf. Sci. 607 (2012) 130–137.
[25] J. Lu, S. Behtash, A. Heyden, J. Phys. Chem. C 116 (2012) 14328–14341.
[26] J. Lu, S. Behtash, M. Faheem, A. Heyden, J. Catal. 305 (2013) 56–66.
[27] A.D. Benavidez, P.D. Burton, J.L. Nogales, A.R. Jenkins, S.A. Ivanov, J.T. Miller, A.M. Karim, A.K. Datye, Appl. Catal. A-Gen. 482 (2014) 108–115.
[28] T.E. Whyte, Catal. Rev. 8 (1973) 117–134.
[29] M.E. Davis, R.J. Davis, Fundamentals of Chemical Reaction Engineering, 1st ed., Dover Publications, Mineola, NY, 2012.
[30] A.L. Patterson, Phys. Rev. 56 (1939) 978–982.

Please cite this article in press as: J.A. Lopez-Ruiz, et al., Appl. Catal. A: Gen. (2015), http://dx.doi.org/10.1016/j.apcata.2015.01.032

[31] H.N. Pham, Y.J. Pagan-Torres, J.C. Serrano-Ruiz, D. Wang, J.A. Dumesic, A.K. Datye, Appl. Catal. A-Gen. 397 (2011) 153–162.

[32] P.B. Weisz, C.D. Prater, Adv. Catal. 6 (1954) 143–196.

[33] H.N. Pham, A.E. Anderson, R.L. Johnson, K. Schmidt-Rohr, A.K. Datye, Angew. Chem. Int. Ed. Engl. 51 (2012) 13163–13167.

[34] E.W. Ping, J. Pierson, R. Wallace, J.T. Miller, T.F. Fuller, C.W. Jones, Appl. Catal. A-Gen. 396 (2011) 85–90.

[35] E.W. Ping, R. Wallace, J. Pierson, T.F. Fuller, C.W. Jones, Microporous Mesoporous Mater. 132 (2010) 174–180.

[36] D.C. Grenoble, M.M. Estadt, J. Catal. 67 (1981) 90–102.

Please cite this article in press as: J.A. Lopez-Ruiz, et al., Appl. Catal. A: Gen. (2015), http://dx.doi.org/10.1016/j.apcata.2015.01.032